Intense and tunable second-harmonic generation in biased bilayer graphene

Søren J. Brun and Thomas G. Pedersen

Department of Physics and Nanotechnology, Aalborg University, DK-9220 Aalborg Øst, Denmark
and Center for Nanostructured Graphene (CNG), DK-9220 Aalborg Øst, Denmark

The centrosymmetric two-dimensional material bilayer graphene (BLG) does not show dipole-allowed second-harmonic generation (SHG) in its pristine form. However, the symmetry can be broken by applying an electric field perpendicular to the layer. Here, we present a theoretical study of SHG from biased BLG. We show that the sheet second-harmonic susceptibility reaches very large values of several hundred nm^2/V in the midinfrared region. The SHG is tunable depending on the strength of the electric field. Furthermore, a strong, tunable double resonance appears in the spectrum. We believe that this study could spark interest in the nonlinear optical properties of biased BLG.

PACS number(s): 42.65.An, 78.20.−e

I. INTRODUCTION

Since the synthesis of graphene in 2004 [1], two-dimensional (2D) materials have attracted tremendous interest. Graphene has been studied widely due to its remarkable electronic [2,3] and optical properties [4]. However, the semimetallic nature of graphene limits its applicability for semiconductor devices. Several methods for creating a band gap are being pursued, including graphene nanoribbons [5–7], periodic gating [8], and graphene antidot lattices [9]. Another promising method is to use biased bilayer graphene (BLG), for which it has been shown both theoretically [10–12] and experimentally [11–15] that it is possible to obtain band gaps of a few hundred meV. In order to create a band gap, an electric field is applied perpendicularly to the graphene plane. This breaks the sublattice symmetry, which induces a tunable band gap depending on the strength of the electric field. The band gap has been measured by several groups, and has shown values up to 250 meV [14]. The linear optical properties of BLG have been studied theoretically by Abergel and Fal'ko [16] by including the strongest interlayer coupling γ_1 in a tight-binding (TB) model. Unlike monolayer graphene, in which the conductivity has a constant value of $\sigma_0 = e^2/4\hbar$ for a broad range of energies [4], the conductivity of BLG shows distinct features at low energies related to the interlayer coupling strength. A particular feature at an energy equal to γ_1 was observed. Nicol and Carbotte [17] included the influence of the chemical potential and a perpendicular electric field in their study. For a chemical potential $\mu \neq 0$, the feature at γ_1 splits in two. For a nonvanishing bias, a semiconducting gap appears in the conductivity for $\mu = 0$. The linear response is thus greatly affected by changes in the bias and chemical potential. Doped BLG was studied experimentally by Kuzmenko *et al.* [18,19] using infrared spectroscopy and compared with a TB model, where skew coupling parameters are included. This showed good agreement, and enabled them to determine the TB parameters of BLG. Furthermore, they report evidence of a gate-induced band gap.

Second-harmonic generation (SHG) has been demonstrated in the 2D materials MoS_2, WS_2, and WSe_2, where it has been used to identify crystal lattice orientation and grain boundaries in a polycrystalline sample [20–25]. This shows that SHG may act as a useful noninvasive characterization method for atomically thin samples. SHG has also been measured from 2D metallic quantum wells having thicknesses ranging from a few to several tens of monolayers and compared with theory, which showed good agreement [26]. Furthermore, SHG in MoS_2 has been calculated and compared to experiments with reasonable agreement [27]. One-dimensional structures such as carbon nanotubes have also been studied theoretically, where the SHG was shown to depend strongly on diameter and chirality [28]. Dipole-allowed even order optical processes require materials that are noncentrosymmetric. Monolayer graphene has inversion symmetry, meaning that it does not show any dipole-allowed SHG. However, it has been shown theoretically that graphene shows SHG when the valley symmetry is broken [29]. Furthermore, SHG from graphene at oblique incidence of radiation has been studied theoretically, showing large values when compared with typical 2D semiconductor structures [30]. Graphene at oblique incidence of radiation has also been studied experimentally, which shows SHG with fourfold symmetry when rotated around the surface normal due to quadrupole optical transitions [31,32]. Taking into account the photon momentum transfer to electron system, it has been demonstrated theoretically that SHG from graphene using linearly polarized light can be strongly circularly polarized [33]. Strong third-harmonic generation (THG) has been measured from monolayer graphene, and it was reported that the SHG from the same sample was two orders of magnitude lower than the THG [34].

Pristine BLG is centrosymmetric, having an inversion point at the midpoint between the layers (cf. the inset in Fig. 1), which means that it will not show strong SHG unless the symmetry of the material is broken, which may be achieved by applying a perpendicular electric field. The nonlinear optical properties of BLG have only been studied to a limited extent. In the low-energy regime, BLG has been shown theoretically to display efficient high harmonic generation [35]. Using a Dirac model description, Wu *et al.* [36] have shown that BLG will show SHG when an in-plane current is included in order to break the symmetry and thereby enable SHG from the material. In their paper, they reported very large and tunable second-harmonic (SH) susceptibilities. They also found that the SH susceptibility is zero when omitting the in-plane current, and argue that the contributions from opposite momenta (K and K' valleys) cancel. In the present paper, we
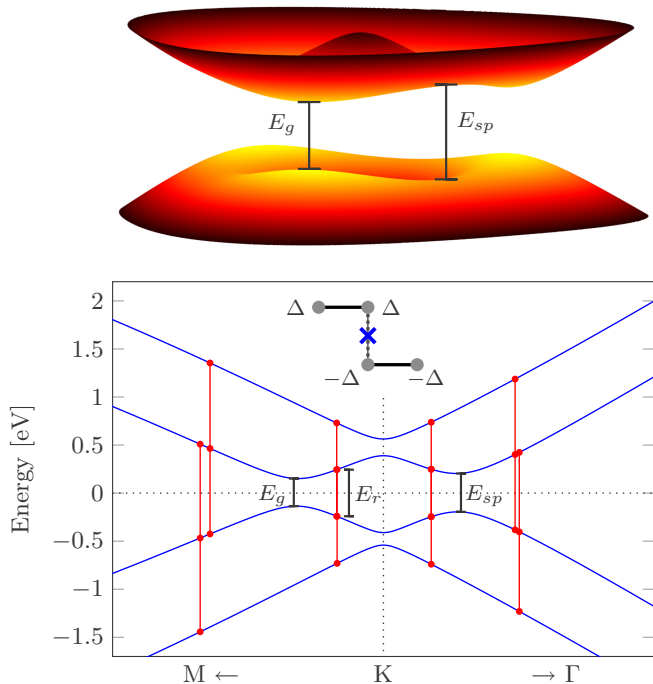
FIG. 1. (Color online) Band structure of biased BLG near the K point for $\Delta = 0.4$ eV. The top part shows the energy surfaces of the top valence band and bottom conduction band near the K point. The bottom part shows the band structure (blue), where double-resonance transitions are shown (red). The inset shows the four-atom unit cell of BLG with shifted on-site potentials. The blue cross marks the inversion point when the electric field is zero.

show analytically that this is indeed the case, but only within the Dirac model. In the full TB model, the K, K' contributions do not cancel, provided a perpendicular electric field is applied. The band gap of BLG can be tuned by varying the applied field, which also affects the SHG as the band structure changes. The band gap reaches values in the midinfrared (MIR) region, where few materials have a strong nonlinear response, thus making BLG a promising platform for nonlinear optical applications.

In this paper, we calculate the SHG in biased BLG using a nearest-neighbor TB model based on the Slonczewski-Weiss-McClure (SWMc) parametrization of graphite [12,37]. For simplicity, we include only the interband contribution to the SH susceptibility. Furthermore, we restrict our analysis to the in-plane response only. The SH response is calculated for different values of the applied bias, which is found to significantly alter the spectrum. We find that the SH susceptibility is nonzero when the perpendicular electric field is nonvanishing. The SH response reaches very large values in the MIR, and a strong double resonance appears at a tunable photon energy depending on the applied electric field. Additionally, we study graphene on hexagonal boron nitride (G/hBN) as an alternative way of breaking the symmetry of graphene. We find that G/hBN shows SHG, although the strength is much weaker than for biased BLG. Finally, we employ an integration method for nonlinear response functions based on the improved triangle method [38]. This method

provides convergence at a much lower k-point sampling, especially near double-resonance transition energies.

II. THEORY AND METHODS

The electronic properties of BLG are well described by a simple TB approach. The band structure of biased BLG has been measured using angle-resolved photoemission spectroscopy, where TB was shown to accurately describe the low-energy properties [13]. In this paper, we employ TB with the SWMc parametrization developed for graphite [12,37]. The Hamiltonian for biased BLG may then be expressed as

$$
\mathbf{H} = \begin{pmatrix} -\Delta - \frac{\Delta'}{2} & -\gamma_0 f(\mathbf{k}) & \gamma_4 f(\mathbf{k}) & -\gamma_3 f^*(\mathbf{k}) \\ -\gamma_0 f^*(\mathbf{k}) & -\Delta + \frac{\Delta'}{2} & \gamma_1 & \gamma_4 f(\mathbf{k}) \\ \gamma_4 f^*(\mathbf{k}) & \gamma_1 & \Delta + \frac{\Delta'}{2} & -\gamma_0 f(\mathbf{k}) \\ -\gamma_3 f(\mathbf{k}) & \gamma_4 f^*(\mathbf{k}) & -\gamma_0 f^*(\mathbf{k}) & \Delta - \frac{\Delta'}{2} \end{pmatrix},
$$

$$(1)$$

where $f(\mathbf{k}) = \exp(ik_x \frac{a}{\sqrt{3}}) + 2\exp(-ik_x \frac{a}{2\sqrt{3}})\cos(k_y \frac{a}{2})$ and $a = 2.46$ Å is the graphene lattice constant. The effect of the bias is incorporated by shifting the on-site potentials of the two layers by $\pm\Delta$. The inset in Fig. 1 shows the four-atom unit cell of BLG with the shifted on-site potentials. The structure is clearly centrosymmetric for $\Delta = 0$ with the inversion point at the blue cross, however, for $\Delta \neq 0$ the centrosymmetry is broken. The SWMc TB parameters for BLG used in our calculations are shown in Table I [37]. Here, γ_0 is the in-plane hopping parameter, γ_1 is the hopping parameter between atoms stacked directly on top of one another, while γ_3 and γ_4 are skew interlayer hopping parameters. Δ' is the difference in on-site potential between atoms stacked on top of each other and atoms above and below hexagon centers.

In order to calculate the SHG, we employ the independent-particle approximation and consider first the limit of low temperatures. The expression for the imaginary part of the sheet SH susceptibility is then [27,28]

$$
\chi_{abc}^{(2)\,\prime\prime}(\omega) = \frac{e^3}{2\pi m_e^3 \hbar^2 \omega^3} \sum_{c,v,l} \int \left[\frac{P_{vcl}}{\omega - \omega_{lv}} \delta(2\omega - \omega_{cv}) \right.
$$
$$
\left. + \left(\frac{P_{vlc}}{\omega + \omega_{cl}} + \frac{P_{clv}}{\omega + \omega_{lv}} \right) \delta(\omega - \omega_{cv}) \right] d^2k, \quad (2)
$$

where $P_{ijl} = \mathrm{Im}\{p_{ij}^a(p_{jl}^b p_{li}^c + p_{jl}^c p_{li}^b)\}/2$, p_{ij}^a is the a component of the momentum matrix element between states i and j, and $\omega_{ij} = \omega_i - \omega_j$. The momentum matrix elements are given by $p_{ij}^a = \mathbf{v}_i^\dagger \mathbf{P_a} \mathbf{v}_j$, where $\mathbf{P_a} = \frac{m}{\hbar} \frac{\partial \mathbf{H}}{\partial k_a}$ is the momentum matrix in the a direction and $\mathbf{v}_i$ is the ith eigenvector. The indices of the sum are restricted such that c runs over all conduction bands, v runs over all valence bands, and $l \neq (c,v)$. If the

TABLE I. TB parameters used for BLG in units of eV.

γ_0	γ_1	γ_3	γ_4	Δ'
3.16	0.381	0.38	0.14	0.022

temperature is nonvanishing, the response function becomes

$$\chi_{abc}^{(2)\,\prime\prime}(\omega) = \frac{e^3}{2\pi m_e^3 \hbar^2 \omega^3} \sum_{c,v,l}$$

$$\int \left[\left(\frac{f_{vl}P_{vcl}}{\omega - \omega_{lv}} + \frac{f_{cl}P_{vcl}}{\omega - \omega_{cl}} \right) \delta(2\omega - \omega_{cv}) \right.$$

$$\left. + \left(\frac{f_{vc}P_{vlc}}{\omega + \omega_{cl}} + \frac{f_{vc}P_{clv}}{\omega + \omega_{lv}} \right) \delta(\omega - \omega_{cv}) \right] d^2k, \quad (3)$$

where $f_{ij} = f_i - f_j$ and f_i is the Fermi occupation factor of state i. An important difference is that the band indices v and c are now unrestricted. All calculations are carried out in the low-temperature limit unless stated otherwise. From symmetry the only nonvanishing elements of the SH tensor are $\chi_{xxx}^{(2)} = -\chi_{xyy}^{(2)} = -\chi_{yyx}^{(2)} = -\chi_{yxy}^{(2)} \equiv \chi^{(2)}$. Note that we consider only the in-plane response of the system. The real part of the SH susceptibility is calculated by Kramers-Kronig transformation. Broadening of the spectra is introduced by convolving with a Lorentzian.

We begin by addressing the finding by Wu *et al.* that the SHG is vanishing when using the Dirac model unless an in-plane current is included. In their paper, they include nearest-neighbor interlayer coupling, such that the Dirac Hamiltonian is

$$\mathbf{H} = \begin{pmatrix} -\Delta & q_- & 0 & 0 \\ q_+ & -\Delta & \gamma_1 & 0 \\ 0 & \gamma_1 & \Delta & q_- \\ 0 & 0 & q_+ & \Delta \end{pmatrix}, \quad (4)$$

where $q_\pm = \hbar v_F (q_x \pm \xi i q_y)$ and $q_{x/y} = k_{x/y} - K_{x/y}$. The parameter ξ determines the K valley ($\xi = +1$ for K and $\xi = -1$ for K'). Changing from K to K' thus corresponds to a complex conjugation of the Hamiltonian, and consequently the eigenvectors are conjugated. We consider the SH tensor element $\chi_{xxx}^{(2)}$, which means that the momentum matrix elements needed are of the type p_{ij}^x. As $\mathbf{P_x}$ is unchanged when conjugated, changing from K to K' entails a complex conjugation of p_{ij}^x, leading to $P_{ijl}(K') = \text{Im}\{(p_{ij}^x)^*(p_{jl}^x)^*(p_{li}^x)^*\} = -P_{ijl}(K)$. This is valid not only at the K,K' points, but for all k points belonging to the K,K' valleys. Contributions to the SH susceptibility from the K valley are thus canceled by contributions from the K' valley. In the TB model used in this paper, the Hamiltonian becomes complex conjugated when changing the k point from $\mathbf{k}$ to $-\mathbf{k}$. However, this does not lead to a complex conjugation of the momentum matrix. Therefore, the analysis from the Dirac model does not apply, and the contributions do not cancel in the TB model.

Other models including, e.g., exciton effects and spin-orbit coupling have also been used for 2D materials such as MoS_2. We neglect spin-orbit coupling, as this effect is very weak in graphene [39]. Exciton effects are also omitted, meaning that the computational effort needed for the calculations is significantly lowered. This enables a more thorough analysis of the effects of the bias as well as other parameters. Moreover, it has been shown that the SH response increases when exciton effects are included [27].

It is well known that applying an electric field perpendicular to BLG opens up a band gap that depends on the magnitude of the electric field [10–15]. The band structure near the K

point calculated using the Hamiltonian in Eq. (1) is shown in Fig. 1, where the shift of the on-site potentials has been set to $\Delta = 0.4$ eV. Experimentally, electric fields up to 3 V/nm, corresponding to $\Delta = 0.5$ eV, have been obtained [14]. The top part of the figure shows the energy surfaces of the top valence band and bottom conduction band near the K point, where the band gap E_g and saddle point transition energy E_{sp} are illustrated. The band structure is shown in the bottom part. Here, the red lines show double resonances in the band structure, which occur at fundamental photon energies E_r where $\omega = \omega_{lv}$ and $2\omega = \omega_{cv}$ are fulfilled simultaneously. Double-resonance transitions generally appear at two energies for biased BLG, in this case at 0.49 and 0.87 eV.

The behavior of the double resonances may be described by considering the simple Dirac model given by Eq. (4). The eigenvalues of this Hamiltonian are

$$E = \pm \frac{1}{\sqrt{2}} \sqrt{2\Delta^2 + \gamma_1^2 + 2q^2 \pm \sqrt{16\Delta^2 q^2 + \gamma_1^4 + 4\gamma_1^2 q^2}},$$

$$(5)$$

where $q^2 = \hbar^2 v_F^2 (q_x^2 + q_y^2)$. The four bands are sorted such that $E_1 < E_2 < E_3 < E_4$, meaning that the resonance condition becomes $E_3 - E_2 = E_2 - E_1$. Solving this for the q closest to the K point leads to

$$q = \frac{1}{4\sqrt{2}} \sqrt{68\Delta^2 + 9\gamma_1^2 - 5\sqrt{144\Delta^4 + 8\Delta^2\gamma_1^2 + 9\gamma_1^4}}, \quad (6)$$

which is only real when $\Delta \geq \gamma_1/\sqrt{8} \simeq 0.135$ eV. Using this value of Δ, the photon energy at which the resonance appears becomes $E_{r,\min} = E_2 - E_1 = \gamma_1/\sqrt{2} \simeq 0.269$ eV.

The integral in Eq. (2) may be calculated numerically using the improved triangle method described in Ref. [38]. For numerical reasons, broadening is introduced through $\hbar\omega \to \hbar\omega + i\Gamma$, where Γ should be small. In the full TB model, the response is generally not divergent at the double resonance except at a few specific energies and is well behaved otherwise. However, as Γ decreases, the integral requires a huge amount of k points for the results to be converged at photon energies near the double resonances. The reason for the slow convergence is that the linearization used in the triangle method becomes inaccurate near the double resonances. We have developed a modified triangle method for nonlinear response functions, in which both the numerator and denominator in the integral are linearized (see the Appendix for the derivation). This method provides converged results at the double resonances without any broadening and at much lower k-point sampling.

III. RESULTS

The SH susceptibility of BLG for selected values of Δ is shown in Fig. 2. The gray dotted lines are located at the energies of $E_g/2$, $E_{sp}/2$, E_g, E_{sp}, and E_r, where special features in the spectra are observed. The SH susceptibility always changes abruptly at $E_g/2$ and E_g, and has van Hove singularities at $E_{sp}/2$ and E_{sp}. It is seen that the susceptibility reaches very large values exceeding 1000 nm²/V for low values of Δ, and several hundred nm²/V at larger values. Such large values are located at photon energies just above
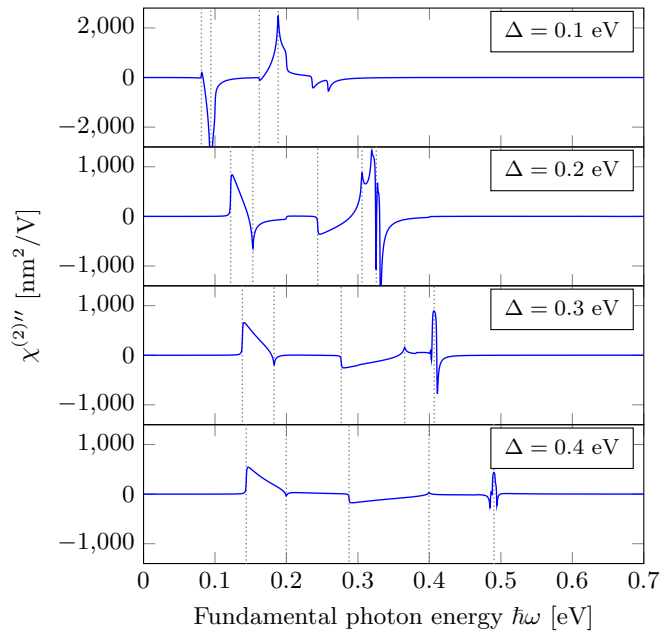
FIG. 2. (Color online) Sheet SH susceptibility of BLG for different values of Δ. The gray dotted lines correspond to (from left to right) $E_g/2$, $E_{sp}/2$, E_g, E_{sp}, and E_r. All spectra have been broadened by 1 meV.

$E_g/2$ and at the double resonance. The first double resonance (the one at the lowest photon energy) shows up very clearly in the three bottom panels. However, no significant features in the spectra are observed at the second resonance. The first resonance is observed in all panels, except for $\Delta = 0.1$ eV,

which is in agreement with the condition derived in Sec. II that $\Delta \geqslant 0.135$ eV is required for the double resonance to appear. Additionally, the resonance is seen to shift to higher energies as Δ increases, while the overall amplitude of the susceptibility decreases.

The TB description of BLG is often approximated by only including the nearest-neighbor in-plane coupling γ_0 and the strongest interlayer coupling γ_1 [10,11,15]. By including the other interlayer coupling parameters, the energy surface at low energies near the K point changes from the Mexican hat dispersion to one with three valence (conduction) band maxima (minima) and three saddle points as shown in Fig. 1. We have found (not shown) that approximating the Hamiltonian by omitting γ_3 and γ_4 from the calculations still produces a nonzero response, but this approximation is too crude for second-order nonlinear optical calculations, as we see notable changes in the SH susceptibility.

Figure 2 shows the SH susceptibility at selected values of Δ. The color plot in Fig. 3 shows the absolute value of the SH susceptibility for varying Δ and fundamental photon energy. At energies below half the band gap, no second-order transitions between valence and conduction bands are possible, and the imaginary part of the SH response is consequently zero in this region. At $E_g/2$, and again at E_g, the susceptibility increases abruptly to very large values, as observed in Fig. 2. The sharp features from the saddle point transition are also easily recognized. At larger energies, the double resonance appears clearly as a sharp line approaching $\Delta = \hbar\omega$. The response is observed to generally be much lower at large photon energies compared with the response at photon energies below ~ 1 eV. From the plot, we note that the double resonance does not extend all the way down to $\Delta = 0$, but only appears at
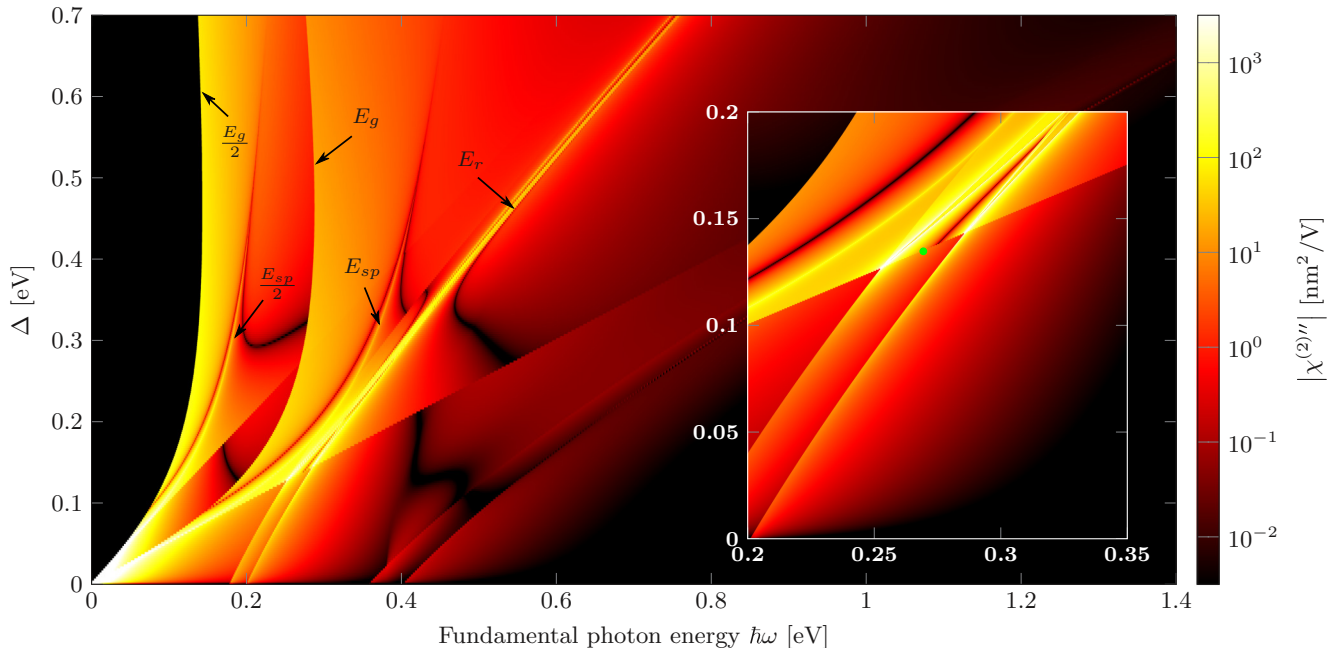

FIG. 3. (Color online) Absolute value of the imaginary part of the sheet SH susceptibility of biased BLG without broadening. The response is exactly zero at photon energies below $E_g/2$. Sharp features from band gap and saddle point transitions appear clearly in the plot. A double resonance appears as an approximately straight line approaching $\Delta = \hbar\omega$. The inset shows a zoom of the region where the double resonance appears. The green dot is at $(\hbar\omega, \Delta) = (\gamma_1/\sqrt{2}, \gamma_1/\sqrt{8})$, which is the analytical prediction of the onset of the double resonance. The color scale has been changed in the inset to enhance the contrast of the double resonance.
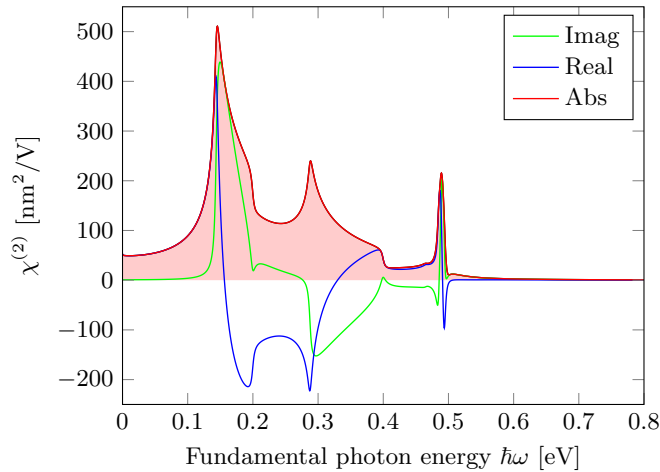
FIG. 4. (Color online) SHG in BLG with the on-site potentials of the two layers shifted by $\Delta = 0.4$ eV. The real part of the SH susceptibility is calculated from Kramers-Kronig transformation. The spectrum is broadened by 5 meV.
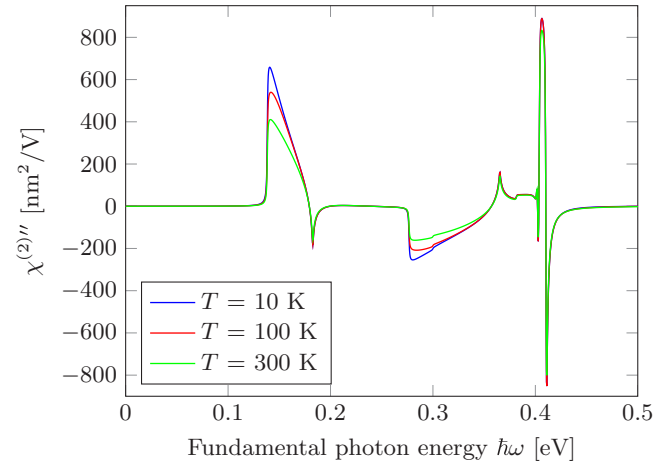

FIG. 5. (Color online) SH susceptibility for $\Delta = 0.3$ eV for different temperatures. The Fermi level is located 10 meV below the conduction band edge. For $T = 10$ K the spectrum is practically identical to the zero-temperature limit. All spectra are broadened by 1 meV.

values of Δ over a certain threshold. This is in accordance with the Dirac analysis in Sec. II, and the inset in Fig. 3 shows a zoom of the region where the resonance appears. The green dot marks the analytical prediction of the onset of the resonance. In this region, the resonance splits in two, and the analytical expression of the onset is seen to be in excellent agreement with the full TB results, as it lies almost perfectly between the onsets of the two branches. From the inset it is also evident that the SH response vanishes as Δ approaches zero, which is expected as the system becomes centrosymmetric in this limit. The results in Fig. 3 clearly show that biased BLG has strong SHG that is tunable by the applied electric field.

The results in Fig. 2 show the imaginary part of the SH susceptibility. The real part may be found by Kramers-Kronig transformation of the spectrum. Figure 4 shows the SHG of BLG with $\Delta = 0.4$ eV where the absolute value of the SH susceptibility is also shown. The spectrum has been broadened by 5 meV. Again, the SHG is seen to reach values of several hundred nm^2/V, and a sharp feature from the double resonance shows up clearly in the spectrum near a photon energy of 0.5 eV.

Next, we study the influence of temperature by calculating the SH susceptibility using Eq. (3). We do this for a fixed electric field given by $\Delta = 0.3$ eV and vary the temperature from zero to room temperature. If the Fermi level is located in the middle of the band gap, the spectrum is nearly unchanged even at high temperatures. The calculated band gap is 276 meV, meaning that the occupancy is only changed slightly even at room temperature. By placing the Fermi level closer to the conduction or valence band, the response becomes more sensitive to temperature changes. Figure 5 shows the temperature dependence of the SH susceptibility for a Fermi level located 10 meV below the conduction band edge. The curve for $T = 10$ K is practically identical to the case of zero temperature. The spectrum changes as the temperature increases, and the features related to the band edge transitions become less dominant, which is expected as this is where the change in occupancy is most significant. However, the double

resonance is related to states at energies further away from the Fermi level, and therefore only minor changes are observed in this part of the spectrum.

As demonstrated above, the optical properties are sensitive to the Fermi level of the system. At Fermi levels intersecting bands in the band structure, the allowed transitions between valence and conduction bands are changed locally (near the K and K' points) due to the Pauli principle, thus changing the optical spectrum. Figure 6 shows examples of the SH susceptibility at different Fermi levels, where the shift of the on-site potentials has again been set to $\Delta = 0.3$ eV. Again, the band gap is 276 meV, meaning that a Fermi level of ± 138 meV will be at the edge of the valence or conduction band. From the figure it is seen that increasing the Fermi level to 0.15 eV only marginally changes the spectrum. The spectrum is only affected in regions caused by transitions near the band gap, i.e., at photon energies just above $E_g/2$ and E_g. However, increasing the Fermi level to 0.2 eV significantly reduces the response, and although the resonance remains, its amplitude is also reduced. Note that the scale bars in the two bottom panels are different from the two top panels. At a Fermi level of 0.25 eV, the response is even lower, and basically no features of the original spectrum remain. The reason for this significant reduction in the response is that when the Fermi level is changed, the occupation at the valence or conduction band edge is changed, and indeed contributions from transitions near the band edges are causing the very high susceptibility.

The absolute value of the zero-temperature SH susceptibility for varying Fermi levels and photon energies is shown in Fig. 7. As expected, the spectrum remains unchanged when the Fermi level is within $\pm E_g/2$. However, as the Fermi level moves into the valence or conduction band, the amplitude of the SH susceptibility is seen to rapidly decrease, although it still displays values of a few nm^2/V. Furthermore, the expected Pauli blockades at slopes of $\pm 1/2$ and ± 1 are observed in the plot. This shows that in order for biased BLG to show strong SHG, the Fermi level should be in the band gap region.
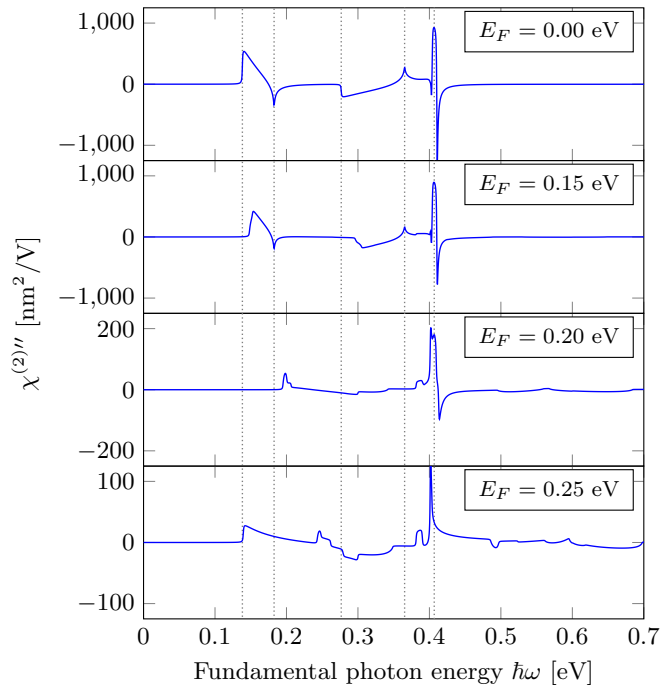
FIG. 6. (Color online) Sheet SH susceptibility of biased BLG using $\Delta = 0.3$ eV for different values of the Fermi level. The gray dotted lines are (from left to right) $E_g/2$, $E_{sp}/2$, E_g, E_{sp}, and E_r of BLG using $\Delta = 0.3$ eV and $E_F = 0$ eV. The spectra are broadened by 1 meV.

An alternative way of breaking the symmetry in a graphene system is by AB stacking a single layer of graphene on top of a single layer of hexagonal boron nitride, forming graphene on hexagonal boron nitride (G/hBN). This creates sublattice
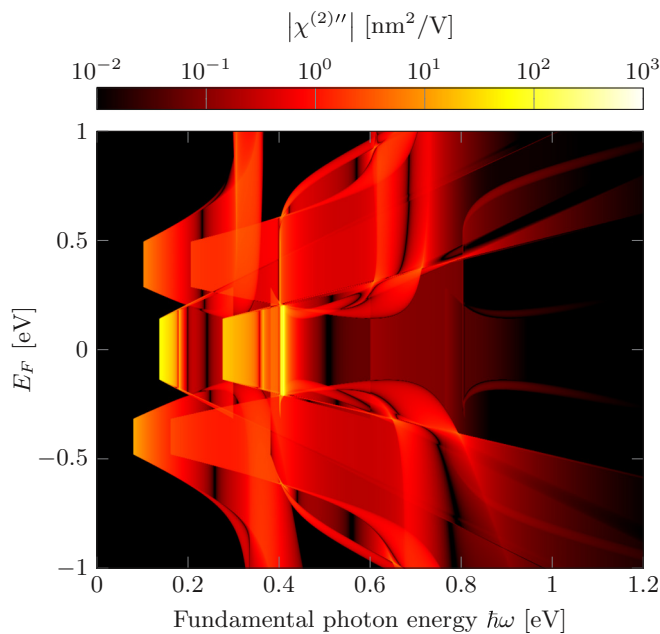

FIG. 7. (Color online) Absolute value of the imaginary part of the sheet SH susceptibility of biased BLG for different Fermi levels using $\Delta = 0.3$ eV. The calculations are made without broadening.
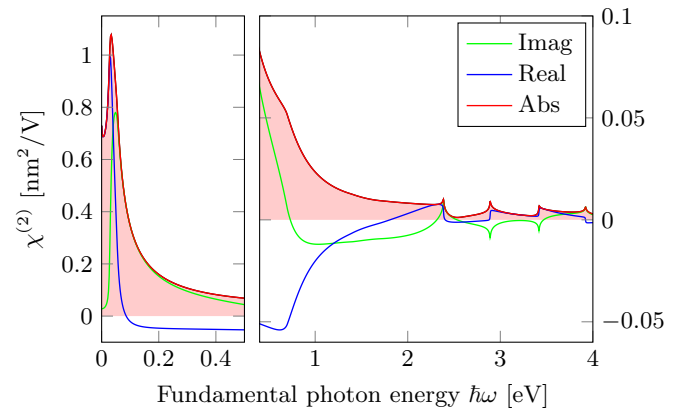

FIG. 8. (Color online) SHG in G/hBN with a broadening of 5 meV. The left part shows the relatively large values at energies close to the band gap while the right part shows the spectrum at larger photon energies.

asymmetry in graphene, making SHG possible. Additionally, a band gap opens up, which has a theoretical value of 53 meV and an experimental value of 31 meV [40,41]. We calculate the SHG from G/hBN using the TB parameters from Ref. [42]. This parametrization only includes the strongest interlayer coupling γ_1. However, we have seen that neglecting the skew coupling parameters strongly affects the SHG, as the system becomes more symmetric. Therefore, we also include the skew coupling parameters from BLG, which should be a good approximation as the two systems are closely related. The SHG from G/hBN is shown in Fig. 8. The left part shows the response at low photon energies, where a peak is observed close to the band gap of the material reaching a value slightly larger than 1 nm^2/V. The right part shows the response at larger photon energies, where the values are much lower than at low photon energies, and only reaches values around 0.01 nm^2/V. This means that G/hBN will show SHG, although the values of the SH susceptibility are orders of magnitude lower than that of biased BLG. The present results demonstrate that SHG can be an excellent probe of the electronic structure of carbon-based 2D materials, similarly to previous studies of metallic 2D materials [26].

IV. CONCLUSION

In this paper, we have presented a theoretical study of SHG from biased BLG using nearest-neighbor TB. When the centrosymmetry is broken by applying a perpendicular electric field, BLG shows a SH response which is tunable by the strength of the electric field. The SH susceptibility reaches very large values, typically several hundred nm^2/V, in the MIR region where few materials show intense SHG. A strong and tunable resonance appears above a certain threshold of the electric field. An analytical estimate of the threshold was shown to be in excellent agreement with the full TB calculations. The SH response is strongly reduced when the Fermi level is moved into the valence or conduction band, although still showing values of a few nm^2/V. We also studied graphene on hexagonal boron nitride, which is another approach to breaking the symmetry of graphene and enabling

SHG. This showed low values of the SH susceptibility at large photon energies and a response around 1 nm^2/V at very low energies, meaning that the response is around two orders of magnitude lower than biased BLG. Additionally, a different triangle integration method capable of handling nonlinear response functions was developed. Due to the very large and tunable SH susceptibility of biased BLG, which also shows a strongly resonant behavior, we believe that this could encourage experimental work on different nonlinear optical graphene-based devices.

ACKNOWLEDGMENTS

APPENDIX: IMPROVED TRIANGLE METHOD FOR NONLINEAR RESPONSE FUNCTIONS

The improved triangle method [38] is useful when integration over a 2D Brillouin zone is required. This method relies on linearization of the k-dependent energies as well as the weight function. The method works well when the weight function is well behaved. However, it struggles to handle singularities in highly nonlinear weight functions. Here, we present a modified triangle method for integrating nonlinear response functions. We consider integrals with weight function F/G of the form

$$
S(\omega) = \int \frac{F(\mathbf{k})}{G(\mathbf{k})} \delta(E_{cv}(\mathbf{k}) - \hbar\omega) d^2k
$$
$$
= \sum_\Delta \int_\Delta \frac{F(\mathbf{k})}{G(\mathbf{k})} \delta(E_{cv}(\mathbf{k}) - \hbar\omega) d^2k = \sum_\Delta S_\Delta(\omega), \quad (A1)
$$

where the integral is divided into a number of triangles denoted by "Δ." By linearizing $E_{cv}(\mathbf{k})$, the integral is rewritten as a line integral along l_Δ where $E_{cv}(\mathbf{k}) = \hbar\omega$, such that each contribution to the sum becomes

$$
S_\Delta(\omega) \simeq \frac{1}{|\nabla_k E_{cv}|} \int_{l_\Delta} \frac{F(\mathbf{k})}{G(\mathbf{k})} dl. \quad (A2)
$$

The functions F and G are then linearized along l_Δ, such that $F = F_a + \frac{l}{L}(F_b - F_a)$, where $F_a = F(\mathbf{k_a})$, $F_b = F(\mathbf{k_b})$, and L is the length of l_Δ. Important k points for the triangle method as well as the integration line l_Δ are shown in Fig. 9. $G(\mathbf{k})$ is
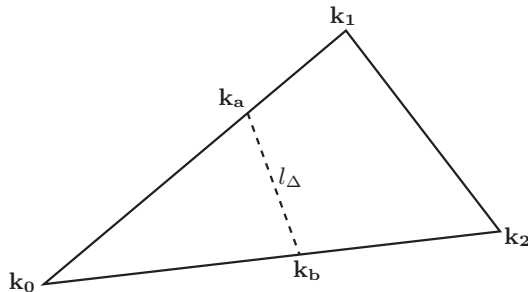
FIG. 9. Important k points for the triangle integration method.

linearized in the same way. The contribution then becomes

$$
S_\Delta(\omega) = \frac{2A_\Delta C}{(G_b - G_a)^2} \Bigg[(F_b - F_a)(G_b - G_a)
$$
$$
+ (F_b G_a - F_a G_b) \ln\left(\left|\frac{G_a}{G_b}\right|\right) \Bigg], \quad (A3)
$$

where A_Δ is the area of the triangle. We use the notation $E_i = E_{cv}(\mathbf{k_i})$ and sort the energies such that $E_0 \leqslant E_1 \leqslant E_2$. The parameters F_a, F_b and C are given by

$$
F_b = F_0 + (\hbar\omega - E_0)\frac{F_{20}}{E_{20}}, \quad (A4)
$$

$$
F_a = \begin{cases} F_0 + (\hbar\omega - E_0)\frac{F_{10}}{E_{10}}, & E_0 \leqslant \hbar\omega < E_1, \\ F_1 + (\hbar\omega - E_1)\frac{F_{21}}{E_{21}}, & E_1 \leqslant \hbar\omega < E_2, \end{cases} \quad (A5)
$$

$$
C = \begin{cases} \frac{\hbar\omega - E_0}{E_{20} E_{10}}, & E_0 \leqslant \hbar\omega < E_1, \\ \frac{E_2 - \hbar\omega}{E_{21} E_{20}}, & E_1 \leqslant \hbar\omega < E_2, \end{cases} \quad (A6)
$$

where $E_{ij} = E_i - E_j$ and $F_{ij} = F_i - F_j$. The parameters for G are calculated similarly.

The effect of using this method is illustrated in Fig. 10, where the SH susceptibility of BLG has been calculated near a double resonance using the normal triangle method and our method. The top part shows the normal method, where a complex frequency $\hbar\omega \to \hbar\omega + i\Gamma$ is required for convergence. The spectra in the bottom part are calculated using the method with $\Gamma = 0$. The figure clearly shows that the method provides converged results using significantly fewer k points compared with the normal triangle method, which requires three orders of magnitude more k points for convergence.
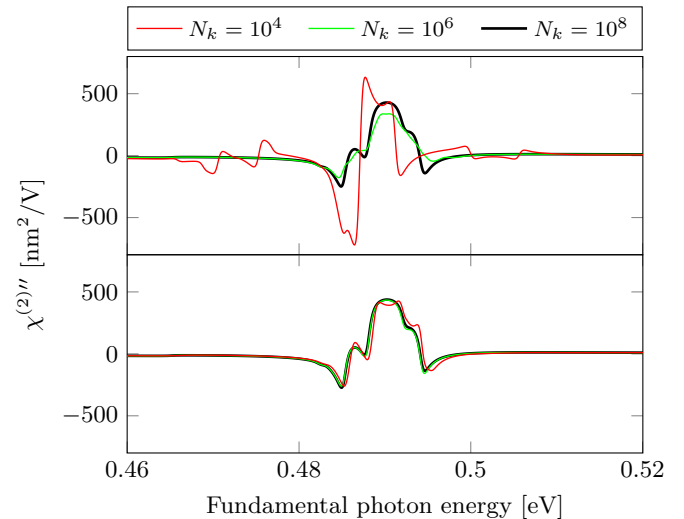
FIG. 10. (Color online) Convergence of the SH response near a double resonance for $\Delta = 0.4$ eV calculated using the normal triangle method (top) and our method (bottom). N_k denotes the total number of k points in the irreducible Brillouin zone. A complex frequency $\hbar\omega \to \hbar\omega + i\Gamma$ with $\Gamma = 0.1$ meV is used for the normal method. After integration, a broadening of 1 meV has been applied to both methods.

It is important to note that this method is only advantageous when the linearization in the regular triangle method is not a good approximation, i.e., near double resonances. In the remaining part of the spectrum, the two methods perform almost equally well. However, double resonances are handled much better using this method where broadening is not required and convergence is obtained using much lower k-point sampling.

[1] K. S. Novoselov, A. K. Geim, S. Morozov, D. Jiang, Y. Zhang, S. Dubonos, I. Grigorieva, and A. Firsov, Science **306**, 666 (2004).

[2] K. Novoselov, D. Jiang, F. Schedin, T. Booth, V. Khotkevich, S. Morozov, and A. Geim, Proc. Natl. Acad. Sci. U.S.A. **102**, 10451 (2005).

[3] K. I. Bolotin, K. Sikes, Z. Jiang, M. Klima, G. Fudenberg, J. Hone, P. Kim, and H. Stormer, Solid State Commun. **146**, 351 (2008).

[4] R. Nair, P. Blake, A. Grigorenko, K. Novoselov, T. Booth, T. Stauber, N. Peres, and A. Geim, Science **320**, 1308 (2008).

[5] B. Obradovic, R. Kotlyar, F. Heinz, P. Matagne, T. Rakshit, M. Giles, M. Stettler, and D. Nikonov, Appl. Phys. Lett. **88**, 142102 (2006).

[6] Y.-W. Son, M. L. Cohen, and S. G. Louie, Phys. Rev. Lett. **97**, 216803 (2006).

[7] M. Y. Han, B. zyilmaz, Y. Zhang, and P. Kim, Phys. Rev. Lett. **98**, 206805 (2007).

[8] J. G. Pedersen and T. G. Pedersen, Phys. Rev. B **85**, 235432 (2012).

[9] T. G. Pedersen, C. Flindt, J. Pedersen, N. A. Mortensen, A.-P. Jauho, and K. Pedersen, Phys. Rev. Lett. **100**, 136804 (2008).

[10] E. McCann, Phys. Rev. B **74**, 161403 (2006).

[11] E. V. Castro, K. Novoselov, S. Morozov, N. Peres, J. L. Dos Santos, J. Nilsson, F. Guinea, A. Geim, and A. C. Neto, Phys. Rev. Lett. **99**, 216802 (2007).

[12] L. Zhang, Z. Li, D. N. Basov, M. Fogler, Z. Hao, and M. C. Martin, Phys. Rev. B **78**, 235408 (2008).

[13] T. Ohta, A. Bostwick, T. Seyller, K. Horn, and E. Rotenberg, Science **313**, 951 (2006).

[14] Y. Zhang, T.-T. Tang, C. Girit, Z. Hao, M. C. Martin, A. Zettl, M. F. Crommie, Y. R. Shen, and F. Wang, Nature (London) **459**, 820 (2009).

[15] K. F. Mak, C. H. Lui, J. Shan, and T. F. Heinz, Phys. Rev. Lett. **102**, 256405 (2009).

[16] D. Abergel and V. I. Fal'ko, Phys. Rev. B **75**, 155430 (2007).

[17] E. Nicol and J. Carbotte, Phys. Rev. B **77**, 155409 (2008).

[18] A. Kuzmenko, E. Van Heumen, D. Van Der Marel, P. Lerch, P. Blake, K. Novoselov, and A. Geim, Phys. Rev. B **79**, 115441 (2009).

[19] A. Kuzmenko, I. Crassee, D. Van Der Marel, P. Blake, and K. Novoselov, Phys. Rev. B **80**, 165406 (2009).

[20] L. M. Malard, T. V. Alencar, A. P. M. Barboza, K. F. Mak, and A. M. de Paula, Phys. Rev. B **87**, 201401 (2013).

[21] N. Kumar, S. Najmaei, Q. Cui, F. Ceballos, P. M. Ajayan, J. Lou, and H. Zhao, Phys. Rev. B **87**, 161403 (2013).

[22] X. Yin, Z. Ye, D. A. Chenet, Y. Ye, K. O'Brien, J. C. Hone, and X. Zhang, Science **344**, 488 (2014).

[23] C. Janisch, Y. Wang, D. Ma, N. Mehta, A. L. Elías, N. Perea-López, M. Terrones, V. Crespi, and Z. Liu, Sci. Rep. **4**, 5530 (2014).

[24] H. Zeng, G.-B. Liu, J. Dai, Y. Yan, B. Zhu, R. He, L. Xie, S. Xu, X. Chen, W. Yao *et al.*, Sci. Rep. **3**, 1608 (2013).

[25] W.-T. Hsu, Z.-A. Zhao, L.-J. Li, C.-H. Chen, M.-H. Chiu, P.-S. Chang, Y.-C. Chou, and W.-H. Chang, ACS Nano **8**, 2951 (2014).

[26] T. G. Pedersen, K. Pedersen, and T. B. Kristensen, Phys. Rev. B **60**, R13997 (1999).

[27] M. L. Trolle, G. Seifert, and T. G. Pedersen, Phys. Rev. B **89**, 235410 (2014).

[28] T. G. Pedersen and K. Pedersen, Phys. Rev. B **79**, 035422 (2009).

[29] L. Golub and S. Tarasenko, Phys. Rev. B **90**, 201402 (2014).

[30] S. Mikhailov, Phys. Rev. B **84**, 045432 (2011).

[31] J. J. Dean and H. M. van Driel, Appl. Phys. Lett. **95**, 261910 (2009).

[32] M. Glazov and S. Ganichev, Phys. Rep. **535**, 101 (2014).

[33] M. Glazov, JETP Lett. **93**, 366 (2011).

[34] S.-Y. Hong, J. I. Dadap, N. Petrone, P.-C. Yeh, J. Hone, and R. M. Osgood, Jr., Phys. Rev. X **3**, 021014 (2013).

[35] H. Avetissian, G. Mkrtchian, K. Batrakov, S. Maksimenko, and A. Hoffmann, Phys. Rev. B **88**, 165411 (2013).

[36] S. Wu, L. Mao, A. M. Jones, W. Yao, C. Zhang, and X. Xu, Nano Lett. **12**, 2032 (2012).

[37] E. McCann and M. Koshino, Rep. Prog. Phys. **76**, 056503 (2013).

[38] T. G. Pedersen, C. Flindt, J. Pedersen, A.-P. Jauho, N. A. Mortensen, and K. Pedersen, Phys. Rev. B **77**, 245431 (2008).

[39] M. Gmitra, S. Konschuh, C. Ertler, C. Ambrosch-Draxl, and J. Fabian, Phys. Rev. B **80**, 235431 (2009).

[40] G. Giovannetti, P. A. Khomyakov, G. Brocks, P. J. Kelly, and J. van den Brink, Phys. Rev. B **76**, 073103 (2007).

[41] C. Woods, L. Britnell, A. Eckmann, R. Ma, J. Lu, H. Guo, X. Lin, G. Yu, Y. Cao, R. Gorbachev *et al.*, Nat. Phys. **10**, 451 (2014).

[42] J. Sławińska, I. Zasada, and Z. Klusek, Phys. Rev. B **81**, 155433 (2010).